DOE/NV/11508–23
UC-703

NEAR-FIELD MODELING IN FRENCHMAN FLAT, NEVADA TEST SITE

prepared by

Karl Pohlmann, Craig Shirley and Roko Andricevic

submitted to

Nevada Operations Office
U.S. Department of Energy

December 1996

Publication No. 45154

DOE/NV/11508–23
UC-703

NEAR-FIELD MODELING IN FRENCHMAN FLAT, NEVADA TEST SITE

prepared by

Karl Pohlmann, Craig Shirley and Roko Andricevic
Water Resources Center
Desert Research Institute
University and Community College System of Nevada

Publication No. 45154

submitted to

Nevada Operations Office
U.S. Department of Energy
Las Vegas, Nevada

December 1996

The work upon which this report is based was supported by the U.S. Department of Energy under Contract #DE–AC08–95NV11508.

ABSTRACT

The U.S. Department of Energy (DOE) is investigating the effects of nuclear testing in underground test areas (the UGTA program) at the Nevada Test Site. The principal focus of the UGTA program is to better understand and define subsurface radionuclide migration. The study described in this report focuses on the development of tools for generating maps of hydrogeologic characteristics of subsurface Tertiary volcanic units at the Frenchman Flat Corrective Action Unit (CAU). The process includes three steps. The first step involves generation of three-dimensional maps of the geologic structure of subsurface volcanic units using geophysical logs to distinguish between two classes: densely welded tuff and nonwelded tuff. The second step generates three-dimensional maps of hydraulic conductivity utilizing the spatial distribution of the two geologic classes obtained in the first step. Each class is described by a correlation structure based on existing data on hydraulic conductivity, and conditioned on the generated spatial location of each class. The final step demonstrates the use of the maps of hydraulic conductivity for modeling groundwater flow and radionuclide transport in volcanic tuffs from an underground nuclear test at the Frenchman Flat CAU. The results indicate that the majority of groundwater flow through the volcanic section occurs through zones of densely welded tuff where connected fractures provide the transport pathway. Migration rates range between near zero to approximately four m/yr, with a mean rate of 0.68 m/yr. This report presents the results of work under the FY96 Near-Field Modeling task of the UGTA program.

CONTENTS

FIGURES

TABLES

INTRODUCTION

Many years of underground nuclear testing at the Nevada Test Site (NTS) has introduced large quantities of radionuclides into the subsurface, including the saturated zone. Some of the radionuclides are readily transported in groundwater and therefore pose a risk of migrating great distances from their sources. The U.S. Department of Energy (DOE) has designated the various source areas on the NTS as Corrective Action Units (CAUs), and many of them will be the focus of detailed investigation of radionuclide transport in groundwater. Frenchman Flat is located above the regional carbonate aquifer (although the hydraulic connection is unclear) and in close proximity to an NTS boundary, thus the Frenchman Flat CAU is one of the first to be investigated.

The high degree of spatial variability resulting from natural geologic heterogeneity is incorporated in the approach utilized here. The availability of hydraulic data in most areas of the NTS is limited, so geophysical data have been used as surrogates to characterize the heterogeneity of hydrogeologic units (Pohlmann and Andricevic, 1994; Shirley *et al.*, 1996). These studies defined various hydrostratigraphic units in the volcanic tuff section and characterized their geometric configurations (thickness, horizontal and vertical continuity). Using this information and data on the spatial characteristics of selected hydraulic properties, hydraulic conductivity can be represented as a spatially-correlated random field. Contaminant transport can then be simulated using a particle-tracking random-walk (PTRW) technique.

This report presents the results of the application of newly-developed tools for generating three-dimensional maps of hydraulic conductivity of the volcanic tuffs at the Frenchman Flat CAU. Although most of the nuclear tests at Frenchman Flat occurred in the valley fill, it is generally thought that migration of radionuclides in groundwater away from the testing areas must first pass through the volcanic section before entering the underlying regional carbonate aquifer. Existence of direct pathways to the carbonates have been postulated, but information about them was insufficient at the time of this study to be incorporated in the model. The hydraulic conductivity maps are used as input for groundwater flow and transport models of radionuclide migration in groundwater from underground nuclear tests at the Frenchman Flat CAU. Modeling is conducted at the scale of one or several shots, which is termed the "near-field" scale. This report is a companion report to Shirley *et al.* (1996), which presents maps of hydrostratigraphic units in northern Frenchman Flat, upon which the conductivity fields presented here are based.

SITE DESCRIPTION

Hydrogeologic Setting

Frenchman Flat is an alluvium-filled closed basin that is elongated along the northeast-southwest axis. The basin is bounded on the south and east by the Ranger Mountains and Mercury Ridge outcrops and on the west by the Hampill Hill-Mount Saylor High (Miller and Healy, 1986). Winograd and Thordarson (1975) describe the four principal hydrogeologic units that are important to groundwater flow below Frenchman Flat. They are the lower carbonate aquifer, the tuff

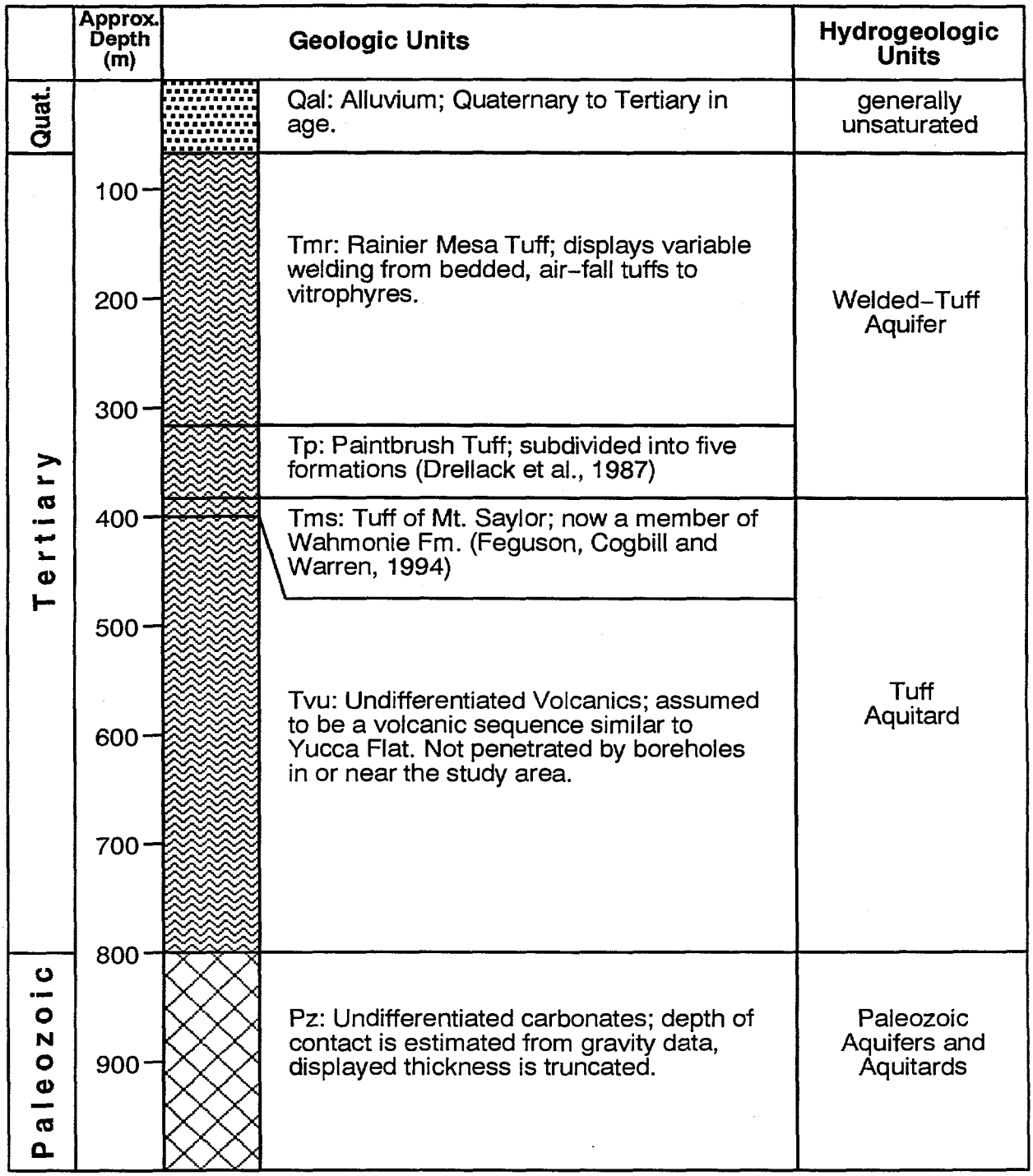

Figure 1. Generalized lithostratigraphic and hydrogeologic columns for the Frenchman Flat CAU.

aquitard, the welded-tuff aquifer, and the valley-fill aquifer. The following summary is based primarily on Winograd and Thordarson's work. Generalized lithostratigraphic and hydrogeologic columns for the Frenchman Flat CAU are shown in Figure 1.

The lower carbonate aquifer is composed of Middle Cambrian through Devonian carbonate rocks, and reaches a saturated thickness of 1000 m or more. The porosity and hydraulic conductivity of the carbonate matrix are both very low, so fractures provide the means for most groundwater flow in the unit. Although the fracture frequency is widely variant, overall fracture conductivity is high enough that the carbonate aquifer is one of the most transmissive on the NTS; the IT/GeoTrans database reports a range of hydraulic conductivities from 0.09 to 731 m/d based on 17 measurements on the NTS (Rehfeldt *et al.*, 1996). The lower carbonate aquifer, which provides for most of the interbasin flow in the regional aquifer system, appears to underlie most of Frenchman Flat.

The tuff aquitard consists primarily of nonwelded to partially-welded ash-flow tuff and ash-fall tuff of Tertiary age. Other rocks included in this unit are tuff breccia, breccia flow, tuffaceous sandstone, siltstone, mudstone, freshwater limestone, and minor densely welded tuff, all of Tertiary age. The tuffs in this unit have been altered *in situ* to zeolites and clays and, thus, exhibit high interstitial porosity but very low interstitial hydraulic conductivity. In addition, since fractures and faults in this friable, nonwelded unit do not remain open and available for groundwater flow, overall hydraulic conductivity is very low. The tuff aquitard is as much as 400 m thick below Frenchman Flat and separates the valley-fill and welded-tuff aquifers from the underlying lower carbonate aquifer.

The welded-tuff aquifer is composed of late Miocene and Pliocene nonwelded to densely welded ash-flow tuff, with minor amounts of ash-fall tuff. Interstitial porosity is inversely related to the degree of welding; nonwelded tuff may exhibit interstitial porosity greater than 0.50 while the interstitial porosity of densely welded tuff is generally less than 0.05. nonwelded tuffs in the welded-tuff aquifer have very low hydraulic conductivity for the reasons previously mentioned. On the other hand, the densely welded ash-flow tuffs, which have very low interstitial porosity and hydraulic conductivity, tend to be brittle, which aids in the formation of joints and fractures. These features tend to remain open after formation, and therefore represent important pathways for groundwater flow. The UGTA database (described by Rehfeldt *et al.*, 1996) reports the range of hydraulic conductivity values for the welded tuff aquifer to be 0.09 to 1.71 m/d based on seven measurements on the NTS. The welded-tuff aquifer is present only in the deepest parts of Frenchman Flat.

The valley-fill aquifer is characterized by alluvial-fan, fluvial, fanglomerate, lakebed, and mudflow deposits in depressions created by post-Pliocence block faulting. Interstitial porosities of over 200 core samples collected from boreholes in northern Frenchman Flat are generally greater than 0.30 (Reynolds Electrical and Engineering Co., 1993a and 1993b). Hydraulic conductivity ranges from 0.30 to 41 m/d based on 14 measurements on the NTS (Rehfeldt *et al.*, 1996). The valley-fill aquifer is present in the central, structurally deepest portion of Frenchman Flat, where the valley-fill/volcanic-tuff contact is below the water table.

Water-level data in the valley are limited, but the available evidence suggests that semi-perched conditions occur between the valley-fill aquifer and the lower carbonate aquifer. Horizontal gradients in the valley fill of northern Frenchman Flat appear to be very low (approximately

$3.0x10^{-4}$). The evidence implies internal drainage in response to the net downward hydraulic gradient and lack of significant horizontal gradients between Frenchman Flat and adjacent valleys. Therefore, groundwater in the valley-fill aquifer is generally thought to pass through the welded-tuff aquifer and tuff aquitard before reaching the regional lower carbonate aquifer. Groundwater could also flow directly into the carbonate aquifer in locations where the volcanic section is absent.

Study Area

The study area is located in the northern portion of the Frenchman Flat CAU, and measures 2200 m north to south and 2600 m east to west (Figure 2). The valley fill ranges in thickness from 58 m at the northern edge to 506 m at the southeastern corner. The valley fill is saturated only in the southern half where the valley-fill/volcanic-tuff contact dips below the water table surface. Six of the seven underground nuclear tests conducted in the area of study were detonated in the valley fill, between 65 and 247 m above the valley-fill/volcanic-tuff contact (Table 1). The seventh test, U11b, was detonated within the volcanic tuff section, approximately 240 m below the valley-fill/ volcanic-tuff contact. All seven tests were conducted in the vadose zone, between 21.9 and 63.4 m above the water table. The volcanic section dips to the south and is estimated to range in thickness from about 500 m at the northern edge to over 700 m at the southern edge. The thicknesses of the volcanic section are based on estimated depths to the Paleozoic carbonates obtained from gravity data (Miller and Healey, 1986) because none of the boreholes in the study area are deep enough to reach the volcanic-tuff/carbonate contact.

TABLE 1. UNDERGROUND NUCLEAR TESTS IN NORTHERN FRENCHMAN FLAT.

Hole Name	Test Name	Date	Geologic Unit	Distance above (+) or below(-) Tuff (m)*	Distance above water table (m)**
U5i	Derringer	9-12-66	Valley Fill	+64.5	50.0
U5k	Milk Shake	3-25-68	Valley Fill	+241.0	21.9
U11b	Pinstripe	4-25-66	Volcanic Tuff	-238.0	63.4
U11c	New Point	12-13-66	Valley Fill	+135.0	57.0
U11e	Diana Moon	8-27-68	Valley Fill	+247.0	56.7
U11f	Minute Steak	9-12-69	Valley Fill	+223.0	35.6
U11g	Diagonal Line	11-24-71	Valley Fill	+73.5	36.5

*Data from DRI Hydrologic Resources Management Program Geologic Data Base
**Based on average water table elevation of 734 m

METHODOLOGY

A framework for describing subsurface heterogeneity using stochastic theory (Delhomme, 1979; Dagan, 1986; Gelhar, 1986) is the most effective way to mathematically account for the high degree of variability typically present in hydrogeologic systems. The most common approach involves generating a set of equiprobable geologic maps conditioned on the available hard data. Contaminant migration is then simulated for each map, resulting in a set of responses (*e.g.*,

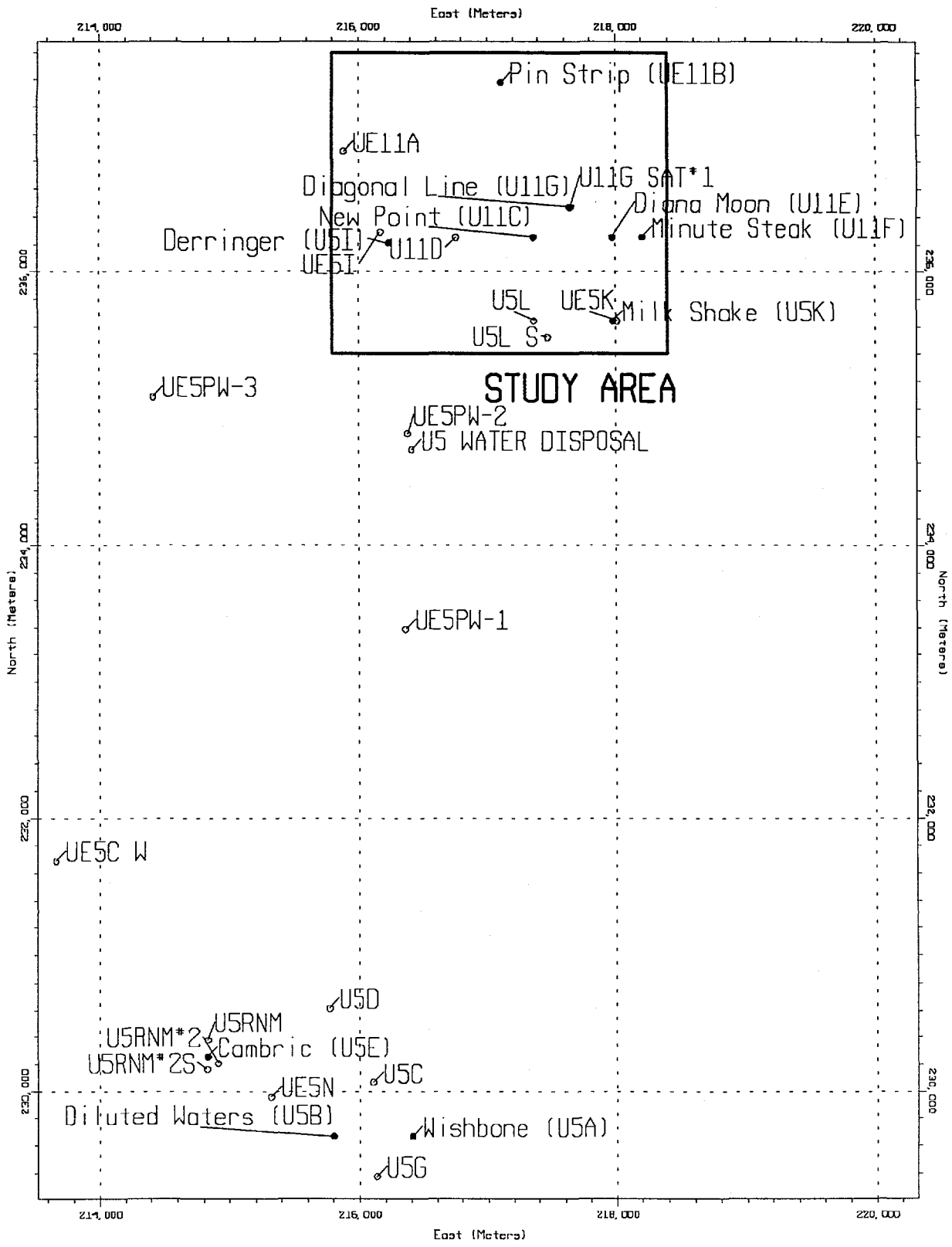

Figure 2. Location of study area in Frenchman Flat, NTS. Locations of boreholes and underground nuclear tests are also shown.

contaminant migration described by breakthrough curves and/or spatial moments) that represents a distribution of equiprobable outcomes.

Pohlmann and Andricevic (1994) present a methodology for generating equiprobable maps of subsurface heterogeneity using all available data while focusing on connectivity patterns of zones having high hydraulic conductivity. The methodology utilizes the sequential indicator simulation (SIS) algorithm to augment sparse hydraulic information with more widely available geophysical information. The SIS algorithm has been implemented as ISIM3D, which is a three-dimensional, multiple indicator, conditional simulation computer program developed by Gomez-Hernandez and Srivastava (1990). Selected borehole geophysical tools (*e.g.*, resistivity, gamma) whose signals demonstrate a correlation to a particular hydrogeologic attribute (*e.g.*, porosity, permeability) are used as conditioning data for the SIS simulations. The continuous range of the geophysical signal is divided into classes, each of which represents a particular category of the hydrogeologic attribute.

Shirley *et al.* (1996) use this methodology to produce three-dimensional geologic maps of two classes of volcanic rocks in the northern portion of the Frenchman Flat CAU. The two geologic classes, nonwelded volcanic tuffs and densely welded ash-fall tuffs, were identified in boreholes using resistivity logs. Resistivity signals have been shown to correlate to the degree of welding in volcanic tuffs on the NTS, which in turn relates to hydraulic conductivity in these rocks (Pohlmann and Andricevic, 1994; Shirley *et al.*, 1996). This relationship can be described as follows: Lithologic logs indicate that most volcanic tuffs at Frenchman Flat are not welded. nonwelded tuffs often exhibit high interstitial porosity, though the pores are only weakly connected and therefore the matrix hydraulic conductivity tends to be very low. nonwelded tuffs generally contain few fractures so the bulk hydraulic conductivity is also very low. These tuffs are less dense than welded tuffs, and their resistivity signals are relatively low. The clay-rich matrices of volcanic tuffs that have undergone alteration processes such as zeolitization cause these rocks to have very low matrix hydraulic conductivities. These tuffs tend to be unfractured as well, so their bulk hydraulic conductivities are also low. Furthermore, the increased ion concentrations of altered rocks reduces their measured resistivity. On the other hand, tuffs that are intensely heated become welded, which reduces matrix porosity and hydraulic conductivity, but often leads to fracturing during cooling or during some other post-depositional process. Interconnected networks of fractures can form significant pathways for groundwater flow, substantially increasing the bulk hydraulic conductivity of welded tuffs. Thus, at the scale modeled in this study, densely welded tuffs tend to be more permeable than nonwelded tuffs, though their matrix porosity is greatly reduced by the welding process. This lower porosity results in greater bulk density and a higher resistivity signal, making densely welded tuffs easily distinguishable from nonwelded and zeolitized tuffs on resistivity logs.

The geologic maps generated by Shirley *et al.* (1996), which are based solely on resistivity logs, describe the spatial distribution of the two classes of volcanic rock, *i.e.*, nonwelded and densely welded tuff, in the study area. Four of the 30 equiprobable realizations of the geologic map are shown in Figures 3 and 4. The shaded areas shown in these figures are cells simulated as densely- welded tuff. The accuracy of the maps depends entirely on the accuracy of the resistivity data used, since no other assumptions are made. Note, however, that the value of the resistivity threshold will

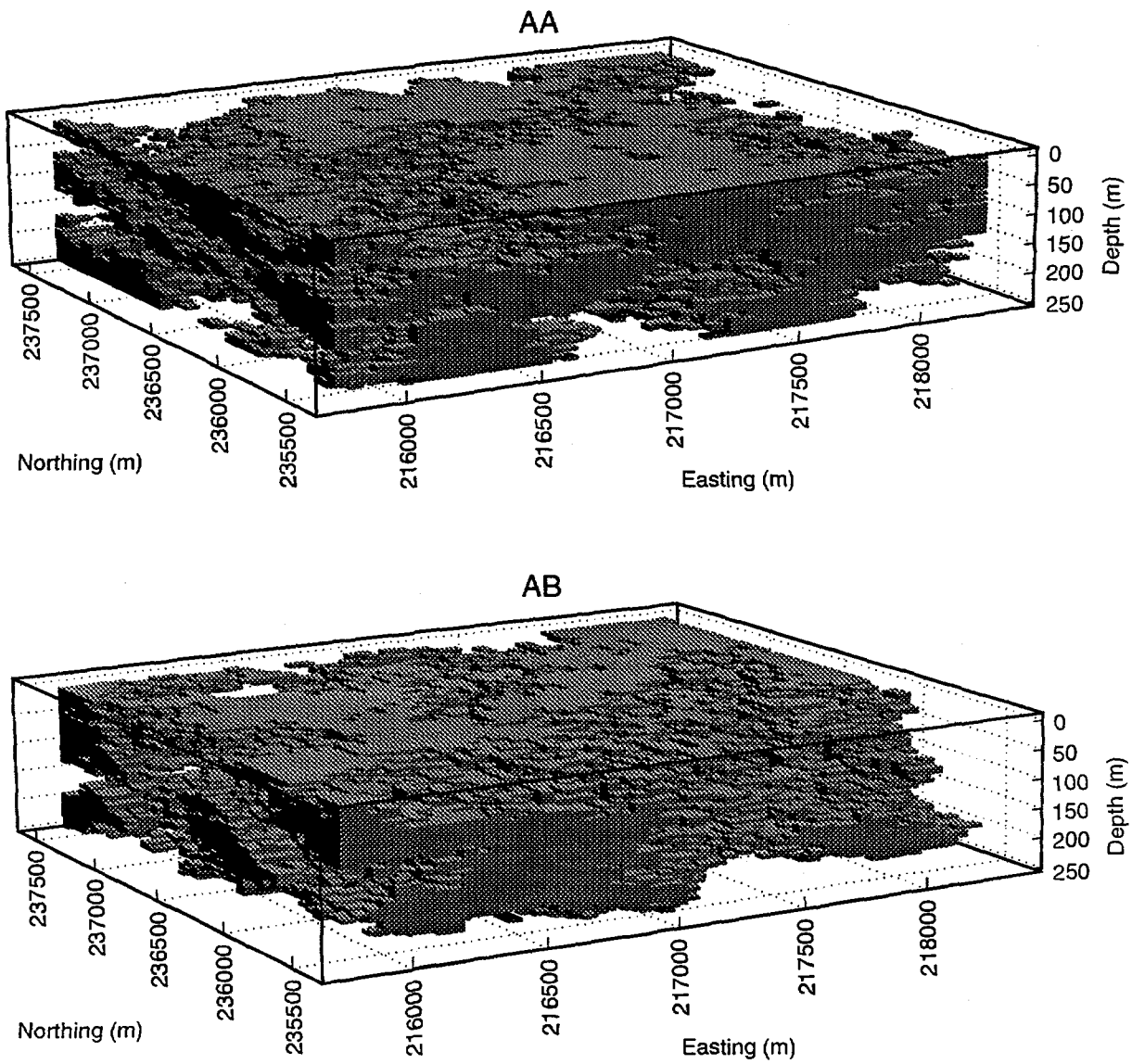

Figure 3. Plot showing realizations AA and AB of the densely welded tuff. The vertical scale represents depth below the top of the volcanic section.

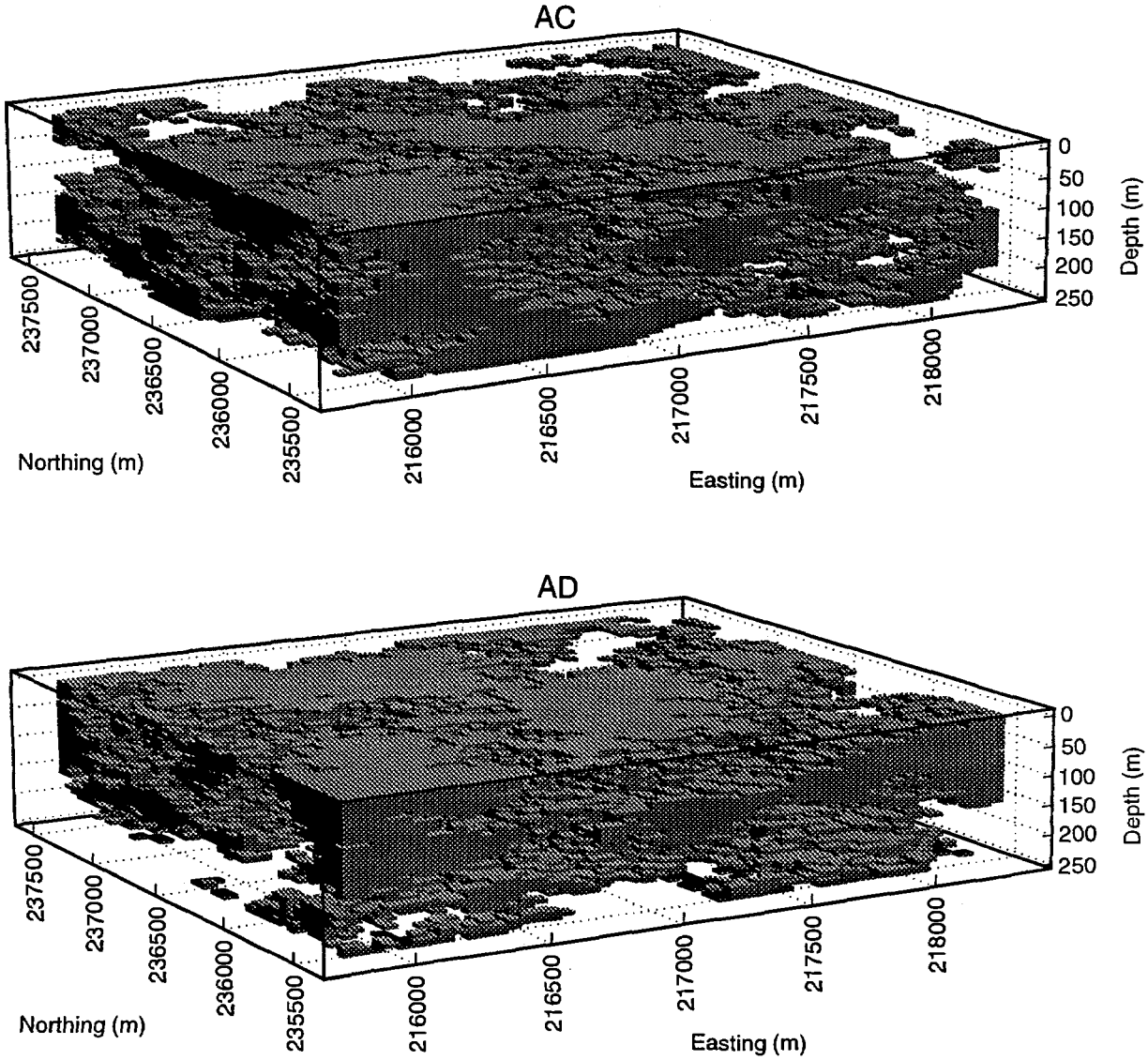

Figure 4. Plot showing realizations AC and AD of the densely welded tuff. The vertical scale represents depth below the top of the volcanic section.

influence the differentiation between the two classes. Blankennagel and Weir (1973) use a resistivity threshold value of 225 ohms-m^2/m to differentiate permeable densely welded tuffs and vitrophyres from relatively impermeable zeolitized tuffs at Pahute Mesa. Drellack (1994) indicates that moderately- to densely welded tuffs at the NTS exhibit resistivity values of 200 to over 1000 ohms-m^2/m. Pohlmann and Andricevic (1994) use a resistivity threshold value of 300 ohms-m^2/m to include only the more densely welded tuffs in the higher class in a study in Yucca Flat. Shirley (1995) concludes that apparent resistivity exceeding 300 ohms-m^2/m is a good geophysical indicator of densely welded tuffs at the NTS.

The geologic maps of the two classes are used as the basis for the three-dimensional maps of hydraulic conductivity. The connectivity of each geologic class, which depends in part on the value of the threshold used, influences the connectivity of potential groundwater flowpaths. The hydraulic conductivity maps are produced using a sequential Gaussian simulation (SGS) alorithm (Deutsch and Journel, 1992). The SGS algorithm generates three-dimensional realizations of a Gaussian process with a given correlation model. The correlation models (one is required for each class) are based on hydraulic information available for each class. In SGS, a random path through the simulation grid is defined such that every node of the grid is visited once. As each node is visited, a predefined search neighborhood is searched for conditioning data, which include both hard data values (if available) and previously simulated values. Simple kriging is used to estimate the value at the current node based on the predefined Gaussian (normal) distribution of the simulation variable. This value is then added to the conditioning data set and the simulation proceeds to the next node.

In this application of SGS, each node of the grid is assigned to one of the two classes that were defined by the SIS simulation. Each class is represented by its own correlation model, which results in a bimodal distribution of hydraulic conductivity, as opposed to the more traditional unimodal distribution. One equiprobable three-dimensional map of the hydraulic conductivity field is generated using SGS for each of the SIS realizations. The hydraulic conductivity maps are then used as the basis for a general flow model to solve for groundwater flux at all nodes, given the gradient of hydraulic head.

Steady-state flux in saturated porous media is described by the Darcy equation:

$$v(x) = -\frac{1}{n(x)}[K(x)\ \nabla\phi(x)] \tag{1}$$

where $v(x)$ is the velocity field, $n(x)$ is the effective porosity field, $K(x)$ is the hydraulic conductivity field, and $\phi(x)$ is the hydraulic head field obtained by solving

$$\nabla \cdot [K(x)\ \nabla\phi(x)] = 0 \tag{2}$$

In this application, fluid density, viscosity, and temperature are considered constant. The mixed hybrid finite element method is employed to discretize Equation (2) and the solution is obtained using the MARFLOW computer program (Mose *et al.*, 1994). The program simultaneously solves

for pressure and flux at each of the six faces of all modeled cells, from which the components of the flux vector for the centroid of each cell are calculated. The fluxes are converted to velocities using the value of effective porosity appropriate for each cell.

Transport of a nonreactive solute in saturated porous media of constant porosity is described by:

$$\frac{\partial c(\boldsymbol{x}, t)}{\partial t} + \nabla \cdot [c(\boldsymbol{x}, t)v(\boldsymbol{x})] - \nabla \cdot [D(\boldsymbol{x}) \nabla c(\boldsymbol{x}, t)] = 0 \tag{3}$$

where $c(\boldsymbol{x},t)$ represents concentration and $D(\boldsymbol{x})$ represents the local hydrodynamic dispersion tensor. The components of $D(\boldsymbol{x})$ are:

$$D(\boldsymbol{x}) = a_T |v(\boldsymbol{x})| I + (a_L - a_T) \frac{v(\boldsymbol{x})v(\boldsymbol{x})}{|v(\boldsymbol{x})|} I + D^* I \tag{4}$$

where a_L and a_T are the longitudinal and transverse local dispersivities, $|v(\boldsymbol{x})|$ is the magnitude of velocity, I is the three-dimensional identity matrix, and D^* is the effective coefficient of molecular diffusion.

Numerical problems such as numerical diffusion and oscillations that are commonly associated with the finite-element solution of Equation (3) can be avoided by utilizing the PTRW method. In the PTRW method, the solute mass is divided evenly between a large number of hypothetical particles that can be located at any point within the domain and that travel at pore-scale velocities. By increasing the number of particles used in the simulation, the solution to Equation (3) becomes more consistent and reliable, and predictions of solute concentrations at specific locations become more accurate. However, the accuracy of the prediction of overall plume behavior does not increase to the same degree. Since average plume behavior is of interest in this study, the total contaminant mass is divided evenly between 10,000 particles.

The velocity fields obtained from the flow model are used as input for the transport simulations; however, since the velocities are known only at the model nodes, an inverse-distance weighting algorithm is used for interpolation of the velocity at the particle location. The dispersion coefficient $D(\boldsymbol{x})$ is considered constant within each cell and is determined from Equation (4). Let $\boldsymbol{x}^p(t)$ represent the position of the pth particle at time t. During each time step Δt, the particle is transported by advective displacement, $\Delta \boldsymbol{x}^p{}_c$ and a dispersive displacement $\Delta \boldsymbol{x}^p{}_d$, such that

$$\boldsymbol{x}^p(t + \Delta t) = \boldsymbol{x}^p(t) + \Delta \boldsymbol{x}^p_c + \Delta \boldsymbol{x}^p_d \tag{5}$$

The deterministic advective displacement is a function of velocity at $\boldsymbol{x}^p(t)$, $v(\boldsymbol{x}^p(t))$, and the gradient of the dispersion tensor at $\boldsymbol{x}^p(t)$

$$\Delta \boldsymbol{x}^p_c = [v(\boldsymbol{x}^p(t)) + \nabla \cdot D(\boldsymbol{x}^p(t))] \cdot \Delta t \tag{6}$$

The gradient terms in Equation (6) are important near hydraulic stagnation points because if these terms are neglected, particles may "build up" in regions of low hydraulic conductivity. In three dimensions, the random dispersive displacement in each time step is

$$\Delta x_d^p = [2D(x^p(t))\Delta t]^{1/2} \cdot z_n \tag{7}$$

where z_n is a realization of a random vector whose size n equals the number of dimensions in the problem. The components of this vector are random values from a standard normal distribution.

The selection of Δt is an important decision in the PTRW simulation process because the computational expense of this method is proportional to the number of time steps. If very short time steps are used, the computational time of the entire simulation may be prohibitive. On the other hand, if excessively large time steps are used, overshoot errors may occur during the solution of Equation (5) (Tompson and Gelhar, 1990). To avoid these problems, Δt should be chosen such that the cell Courant number, C_c, which is the ratio between the average convective displacement and the grid spacing, is less than unity:

$$C_c = \frac{\overline{v(x)} \cdot \Delta t}{\Delta x} \tag{8}$$

where $\overline{v(x)}$ is the mean pore-water velocity. Use of time steps that results in C_c being greater than one may result in overshoot problems.

Radioactive decay of tritium is incorporated in the transport calculations through application of the expression for the first-order decay reaction

$$C = C_0 \exp\left(-\frac{\ln 2}{\omega} t\right) \tag{9}$$

where C is the decayed concentration, C_0 is the undecayed concentration, ω is the half life of tritium in years, and t is time.

It should be noted, however, that including radioactive decay in the transport calculations has the effect of removing the longer travel times from the distribution of breakthrough times. This occurs because tritium, with a short half-life of 12.3 years, that is traveling at very low velocities decays away before reaching the breakthrough plane. Removal of the longer travel times means that the breakthrough curves do not conserve the initial mass. To compare the breakthrough curves from different realizations, each one is normalized with the total mass that crossed the breakthrough plane during that realization.

Tritium plume migration is described in terms of the tritium breakthrough curve crossing a control plane placed at an appropriate distance downgradient from the source location. The tritium breakthrough curve is statistically evaluated using many aquifer realizations by superimposing the center of mass of each realization of the breakthrough curve at the ensemble mean travel time (Andricevic and Cvetkovic, 1996, Figure 1). This procedure describes the relative dispersion and provides the tritium breakthrough curve that includes actual spreading due to velocity fluctuations on the scale smaller than the plume size, and removes the meandering of the plume as a whole which

results from the large scale velocity fluctuations. The ensemble breakthrough curve obtained in this way is more likely to be the one observed with measurements in the field, as opposed to a single breakthrough curve resulting from a single aquifer realization.

APPLICATION, RESULTS AND DISCUSSION

The hydrogeologic setting of northern Frenchman Flat was treated as a three-dimensional system comprised of nonwelded and densely welded Tertiary volcanic tuffs. The volcanic section is treated as a single structural block which is roughly tabular in shape and dips to the south (Shirley *et al.*, 1996). Groundwater flow and transport were considered within the volcanic section only.

The hydraulic conductivity maps are based on the 30 realizations of the subsurface geologic map of nonwelded and densely welded tuffs simulated by Shirley *et al.* (1996), and the available hydraulic conductivity data. Hydraulic conductivity for these tuffs is assumed to be log-normally distributed (Freeze and Cherry, 1979; Hoeksema and Kitinidis, 1985). Using SGS, each of the two classes is represented by its own correlation model of hydraulic conductivity. Because measurements of hydraulic conductivity were not available for northern Frenchman Flat, global estimates of $\mu_{\ln K}$ and $\sigma_{\ln K}$ for each class are estimated from NTS-wide data available in the UGTA database (described by Rehfeldt *et al.*, 1996). To best match the scale of these flow and transport simulations, only K data from pumping tests and recovery tests were used; bail, injection, swab, slug, and laboratory data were excluded. Data for the Welded Tuff Aquifer (WTA) hydrostratigraphic unit are used to represent densely welded tuffs and data for the Tuff Confining Unit (TCU) are used to represent the nonwelded tuffs. The values used to generate realizations of the hydraulic conductivity field are shown in Table 2. The values of $\sigma_{\ln K}$ are estimated from the total range of K values for each unit by dividing the range by four. This approximation assumes that the sample range represents 95.4% of the population or $\pm$ two standard deviations about the mean. This estimate can be refined as new data on the hydraulic conductivity of volcanic tuffs are collected and analyzed.

The correlation structure of K in the volcanic tuffs is not yet well understood, so the values of the correlation lengths, λ_x, λ_y, and λ_z for each class were chosen to be consistent with the values used in the SIS simulations, where λ_x and λ_y equaled 600 m. The spatial correlation of K within each class is expected to be less than the correlation between classes, and the values of λ_x, λ_y, and λ_z reflect this. Because the correlation structure of K is critical to flow and transport, use of different values of correlation length will affect the results. Again, these estimates can be refined as more data are collected within Frenchman Flat and knowledge of the hydrogeologic parameters increases.

The configuration of the SGS grid is identical to that used for the SIS simulations. Horizontal node spacing is 50 m and vertical node spacing is 5 m. Overall grid dimensions are 2550 m in the x (east-west) direction, 2050 m in the y (north-south) direction, and 250 m in the z (vertical) direction. Distances in the z direction represent depth below the top of the volcanic section. Thirty realizations of the hydraulic conductivity field have been produced, one for each SIS realization.

Displaying the regions of a single realization that have hydraulic conductivity higher than a series of selected thresholds is a convenient way to display the three-dimensional connectivity of

TABLE 2. VALUES OF PARAMETERS USED TO GENERATE HYDRAULIC CONDUCTIVITY FIELDS.

Parameter	Value	Source
densely welded tuff		
Mean, $\mu_{\ln K}$	-0.40 (ln m/d)	WTA of Rehfeldt et al., 1996
Standard deviation, $\sigma_{\ln K}$	0.73 (ln m/d)	See text
Correlation scale, $\lambda_x, \lambda_y, \lambda_z$	100, 100, 40 m	See text
nonwelded tuff		
Mean, $\mu_{\ln K}$	-8.42 (ln m/d)	TCU of Rehfeldt et al., 1996
Standard deviation, $\sigma_{\ln K}$	1.66 (ln m/d)	See text
Correlation scale, $\lambda_x, \lambda_y, \lambda_z$	60, 60, 60 m	See text

hydraulic conductivity. The cells of one SGS realization that have hydraulic conductivity values greater than 2.0, 1.5, 0.67, and 0.1 m/d are shown in Figures 5 through 8, respectively. The vertical scale of these figures is depth below the top of the volcanic section. These figures show the configuration and continuity of zones at various levels of conductivity, and clearly exhibit the potential flowpaths that are expected within natural geologic formations. For example, regions having conductivity greater than 2.0 m/d do not appear to extend horizontally over distances greater than a few hundred meters. Vertically, these regions extend less than a few tens of meters. However, the regions having the highest conductivity (*i.e.*, greater than 2 m/d) represent the flowpaths through which the fastest migration of radionuclides may occur. Regions having conductivity greater than 1.5 m/d extend over longer distances, and show increasing continuity when both vertical and horizontal extents are combined. That is, these regions are not necessarily flat-lying: they undulate vertically and horizontally, which has the effect of increasing their extents. Finally, regions having conductivity greater than 0.67 m/d, which is the geometric mean of the densely welded tuff class, extend across the entire domain in both the horizontal and vertical directions. These continuous regions of relatively high conductivity, which extend thousands of meters horizontally and up to approximately one hundred meters vertically, represent the most likely general pathways for groundwater flow and transport.

Another important feature evident on these figures is the anisotropy of the conductive zones. As noted above, the most conductive zones exhibit much greater extent horizontally than they do vertically. This pattern, which results from the anisotropic covariance structure of the subsurface geology, illustrates the spatial anisotropy typically exhibited by volcanic tuff units (Istok *et al.*, 1994). Anisotropy of K within the geologic classes is controlled by the estimated anisotropy of the correlation scales of hydraulic conductivity. No data are available on the anisotropy of K within individual cells.

It is also important to recognize that these three-dimensional simulations provide a more accurate representation of subsurface variability than two-dimensional simulations. The third dimension

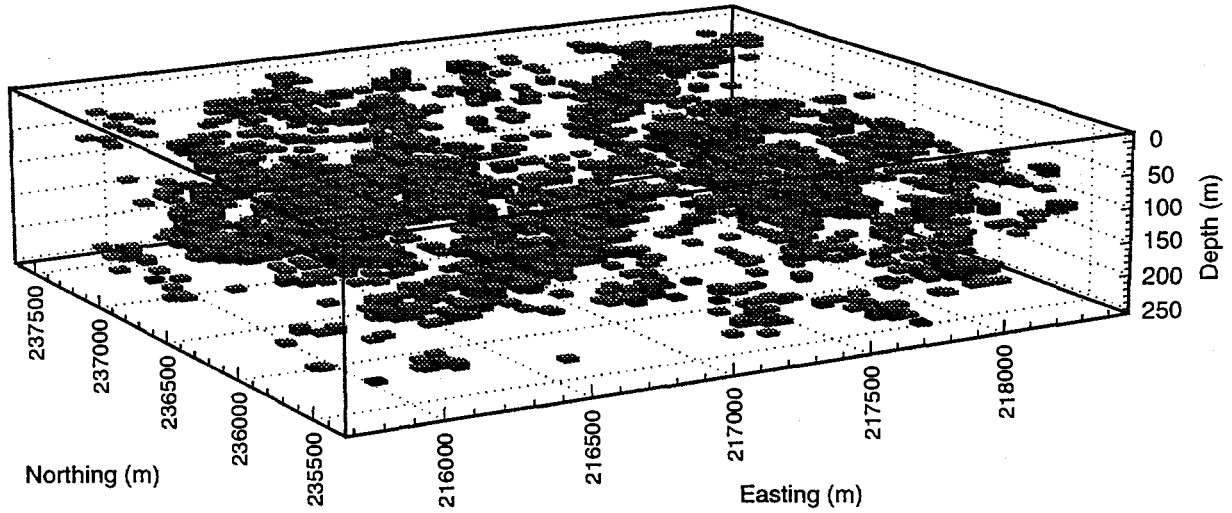

Figure 5. Plot showing cells having hydraulic conductivity greater than 2.0 m/d. The vertical scale represents depth below the top of the volcanic section.

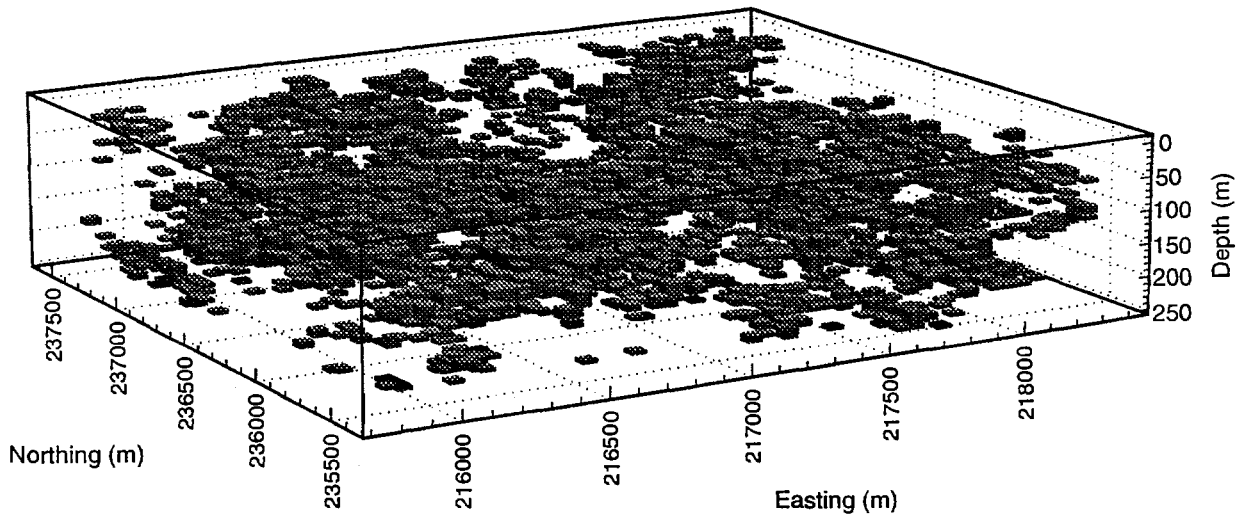

Figure 6. Plot showing cells having hydraulic conductivity greater than 1.5 m/d. The vertical scale represents depth below the top of the volcanic section.

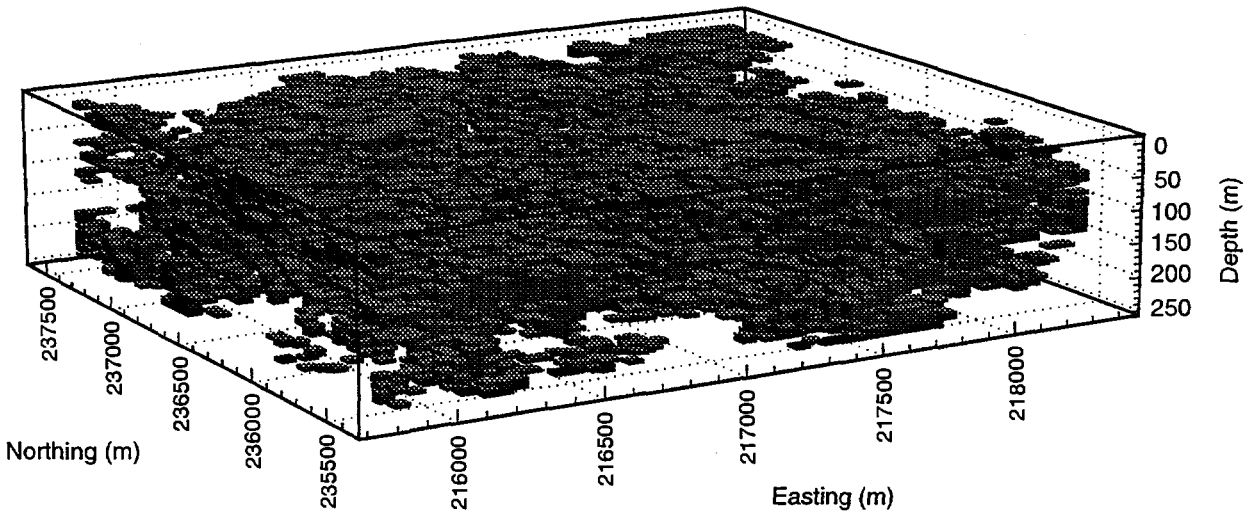

Figure 7. Plot showing cells having hydraulic conductivity greater than 0.67 m/d. The vertical scale represents depth below the top of the volcanic section.

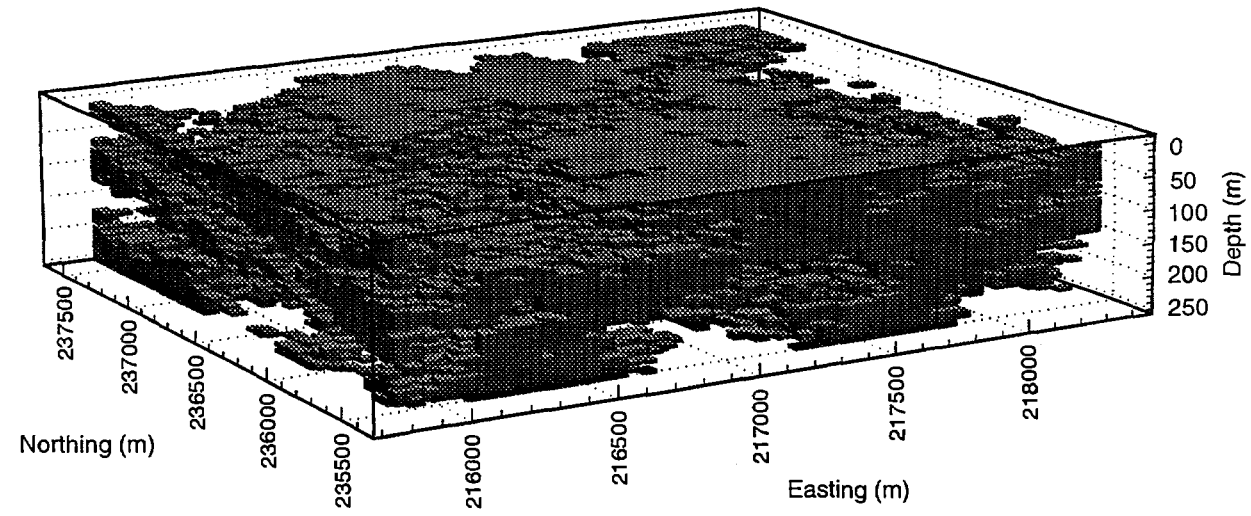

Figure 8. Plot showing cells having hydraulic conductivity greater than 0.1 m/d. The vertical scale represents depth below the top of the volcanic section.

provides the ability for increased connectivity in space that is not possible in a two-dimensional representation. Therefore, the connectivity patterns of groundwater flowpaths must be simulated and evaluated as three-dimensional volume data, just as they exist in real hydrostratigraphic units.

The differences between realizations of the hydraulic conductivity fields are shown for four separate realizations in Figures 9 through 12. All four realizations were simulated using identical known conditioning data (in the SIS simulation) and spatial correlation structure; therefore, all four are equally probable representations of the distribution of hydraulic conductivity. The differences between these realizations result from the prevailing spatial uncertainty, particularly when a small amount of conditioning data are found in the search neighborhood. In the case of Frenchman Flat, few initial conditioning data are available (there are only four wells with useful resistivity data in the model domain), so there is variability between the realizations. The mixed hybrid finite element code MARFLOW (Mose *et al.*, 1994) is used to compute the steady-state groundwater flux field for each realization of the hydraulic conductivity field. Both the domain size and the discretization are maintained from the SIS and SGS simulations. The configuration of the physical domain used for the flux simulations, and the subsequent transport simulations (described below), is shown in Figure 13.

A hydraulic gradient of 0.001 oriented directly south is produced by specified constant head boundaries at the north and south faces of the model domain. This is a maximum gradient based on water levels reported in wells in northern Frenchman Flat. The east, west, upper, and lower faces of the domain are no-flow boundaries. Cell-to-cell fluxes calculated by MARFLOW are converted to velocities using the value of effective porosity appropriate for the class to which that cell belongs. Cells in the welded-tuff class are assigned an effective porosity value of 0.005 (Blankennagel and Weir, 1973, p. 26), and cells in the nonwelded tuff class are assigned a value of 0.01 (Winograd and Thordarson, 1975, p. 118).

The 30 three-dimensional fields of groundwater velocities are used as input to the PTRW code to simulate transport of tritium. The values of the transport parameters used in the PTRW simulations are listed in Table 3. Source-term information is estimated using relationships described by Glasstone and Dolan (1977), with the cavity radius equal to the depth of burial multiplied by 0.0875, and the chimney radius equal to the cavity radius multiplied by 1.2. These relationships were applied for the Pinstripe (U11b) underground nuclear test, which was detonated 296 m below ground surface, giving a chimney radius of 31 m. The initial tritium mass is calculated using the chimney size and a representative tritium concentration (3.3×10^8 pCi/L) for chimney areas on the NTS, exclusive of Pahute Mesa. The source is simulated as a box having edge dimensions corresponding to the chimney diameter, or 62 m. The center of the source is located 250 m downgradient from the upgradient boundary and midway between the top and bottom boundaries to prevent migration of particles out of the domain in these directions. This location places the source below the water table, thereby releasing tritium directly to the saturated zone, although the Pinstripe test actually took place about 63.4 m above the water table. This approximation is reasonable considering the probable extension of the cavity to within 30 m of the water table, and represents a conservative approach to migration. If migration times from the cavity to the water table are long, the downgradient

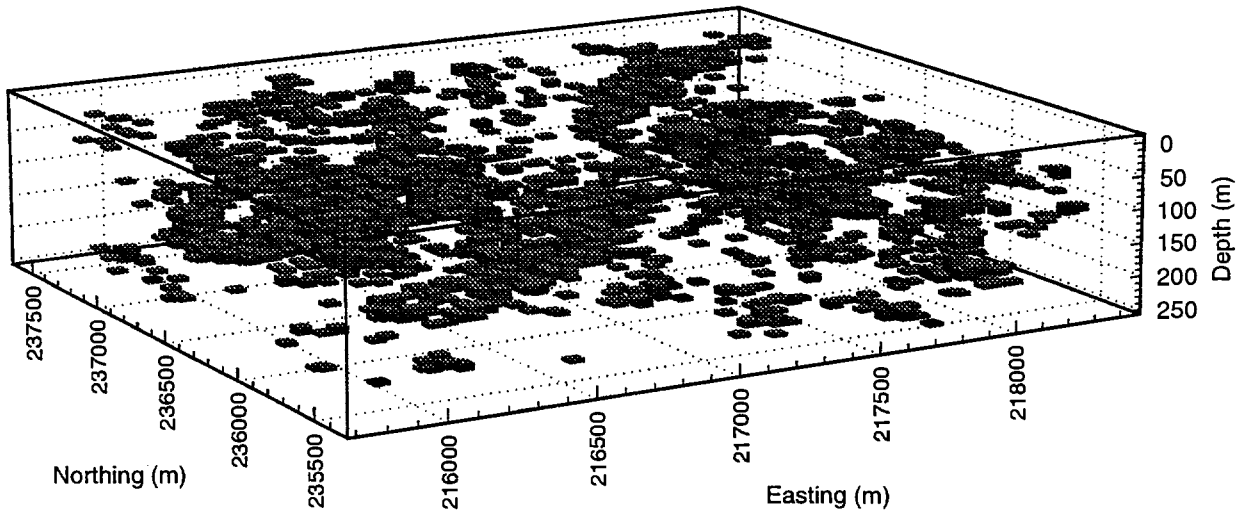

Figure 9. Plot showing cells having hydraulic conductivity greater than 2.0 m/d for realization AA. The vertical scale represents depth below the top of the volcanic section.

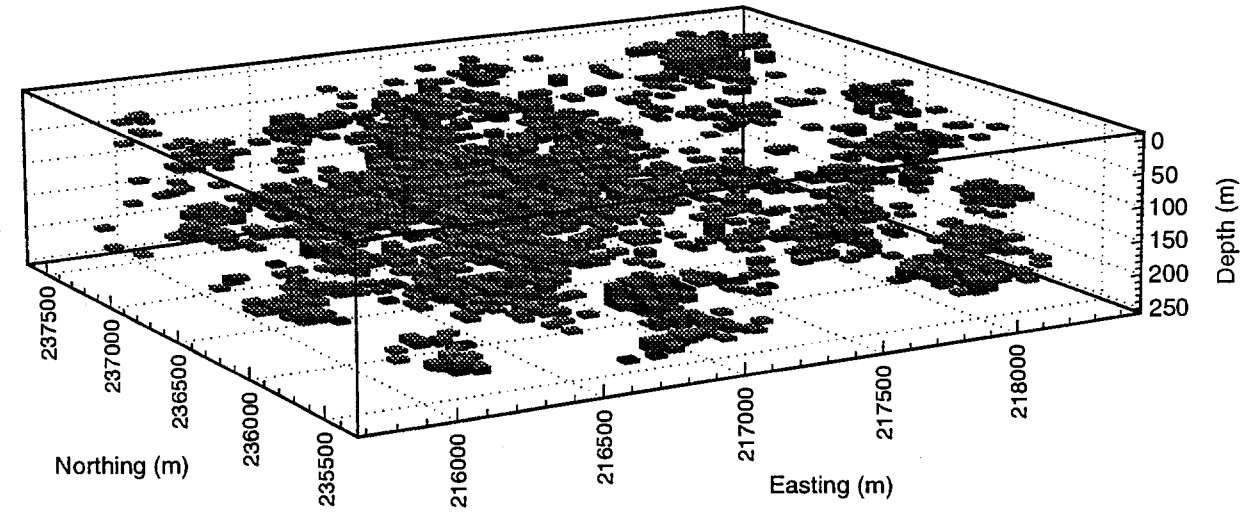

Figure 10. Plot showing cells having hydraulic conductivity greater than 2.0 m/d for realization AB. The vertical scale represents depth below the top of the volcanic section.

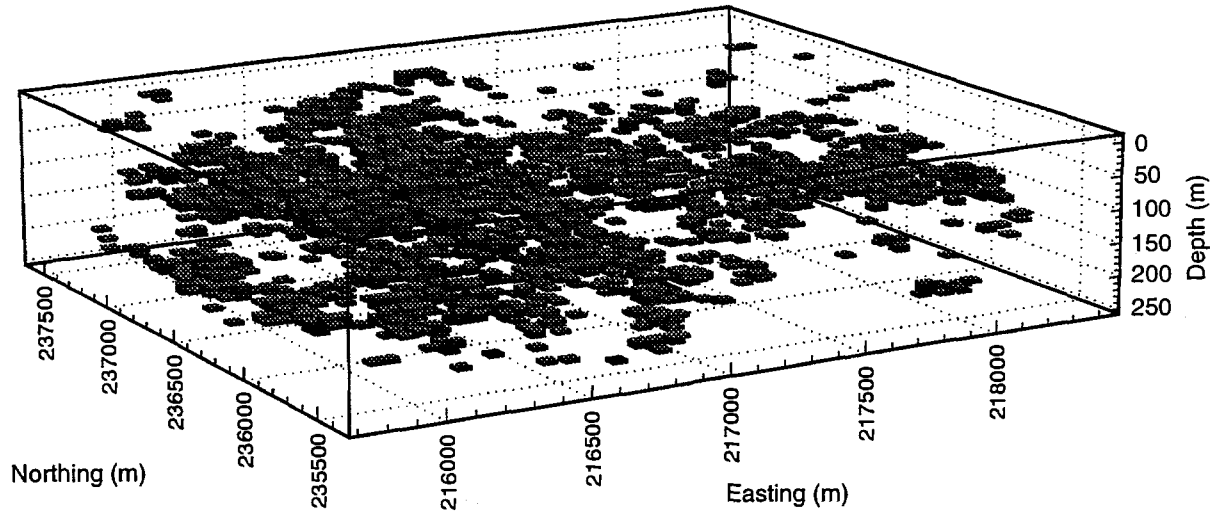

Figure 11. Plot showing cells having hydraulic conductivity greater than 2.0 m/d for realization AC. The vertical scale represents depth below the top of the volcanic section.

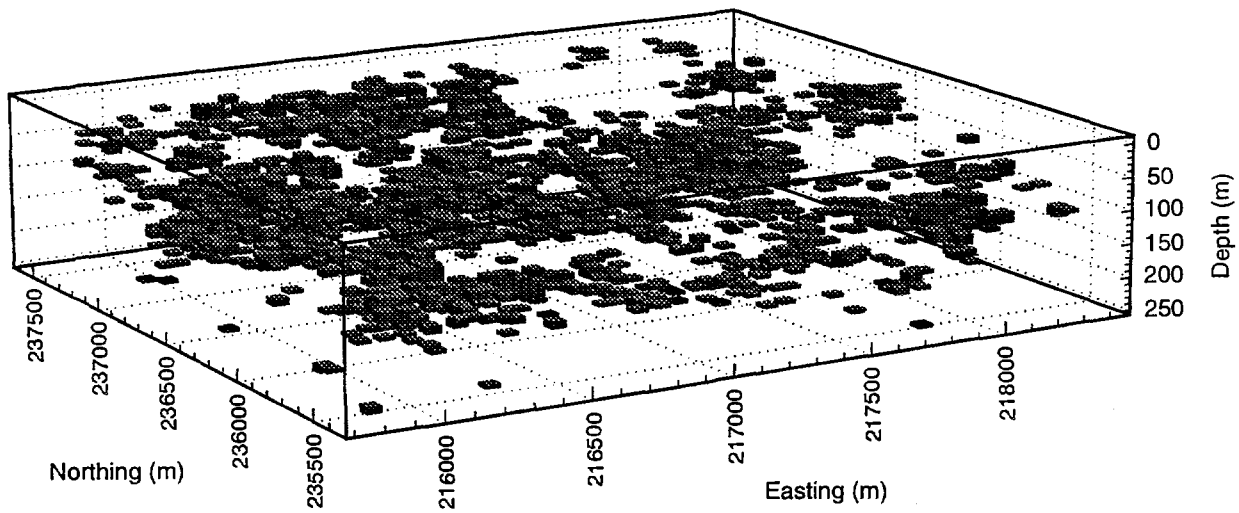

Figure 12. Plot showing cells having hydraulic conductivity greater than 2.0 m/d for realization AD. The vertical scale represents depth below the top of the volcanic section.

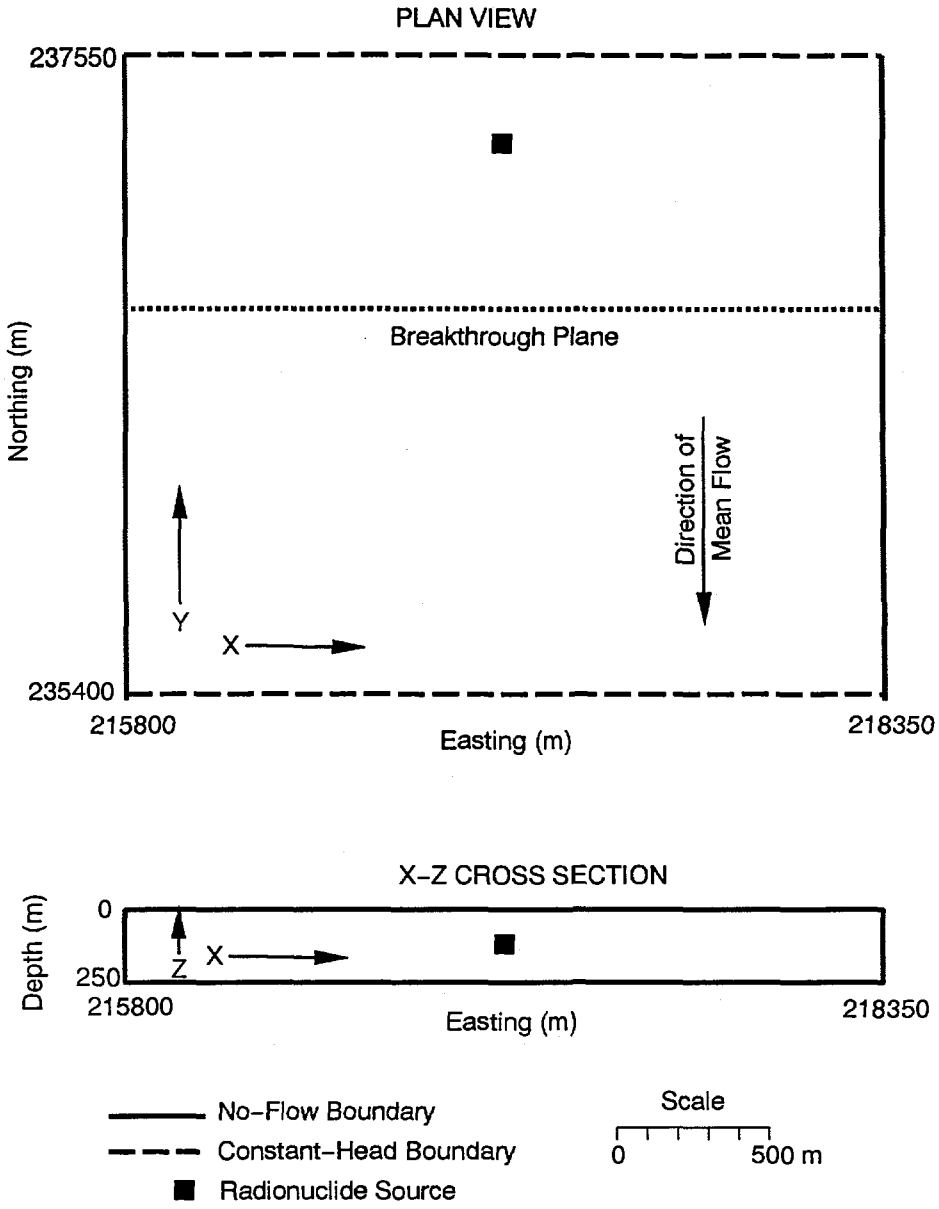

Figure 13. Configuration of the physical domain for flux and transport simulations. The X direction represents east, the Y direction represents north, and the Z direction represents depth below the top of the volcanic section.

breakthrough curves would arrive later and have lower peaks than those presented here. All tritium was assumed to be instantaneously released at t_0 with a unit mass of 1.0 divided evenly between 10,000 particles.

TABLE 3. VALUES OF PARAMETERS USED IN TRANSPORT SIMULATIONS. The text describes how these values were chosen.

Parameter	Value
Source mass	1.0
Source diameter	62 m
Source location (x,y,z)	1275, 1900, 125 m
Number of particles	10,000
Time step	0.5 yr
Total simulation time	275 yr
Longitudinal dispersivity, α_L	1.0 m
Transverse dispersivity, α_T	0.1 m
Diffusion, D^*	0.0
Adsorption rate coefficient, K_1	0.0
Desorption rate coefficient, K_2	1.0
Half life, Tritium	12.3 yr

Radioactive decay is included using the tritium half life of 12.3 years. Adsorption/desorption processes are not included in the simulations because tritium is considered non-reactive and this represents the most conservative approach. Molecular diffusion is assumed negligible and is not included. All simulations are run for 275 years after release, which is the time that tritium at the source is calculated to decay to the EPA human consumption limit of 20,000 pCi/L. To prevent the overshoot errors that may occur if time steps are too long (Tompson and Gelhar, 1990), the time step length was chosen such that the cell Courant number was less than one. All realizations are run using a uniform time step length of 0.5 years. The microscopic dispersivity values, α_L and α_T, are based on values considered appropriate for the scale of the simulation. Note, however, that microscopic dispersion is on a scale much smaller than the cell size and is minimal compared to the macrodispersion caused by the heterogeneous flow field.

The heterogeneous flow field results in a wide range of distances traveled by the centers of plume mass in the 275-year simulation time (Figure 14). The mean distance traveled for all realizations is 188 m, which corresponds to an average migration rate of 0.68 m/year. The median value, which divides the distribution in half, of 35 m gives an average migration rate of 0.13 m/year. It should be noted that these distances are in three-dimensional space, and so incorporate meandering in the vertical and transverse direction, as well as migration in the direction of mean flow.

Because the volume of the simulated source is larger than the volume of individual cells, the source covers cells for which geophysical conditioning data were not available. As a result, the hydraulic conductivity, and sometimes the geologic class, of cells at and near the source differs

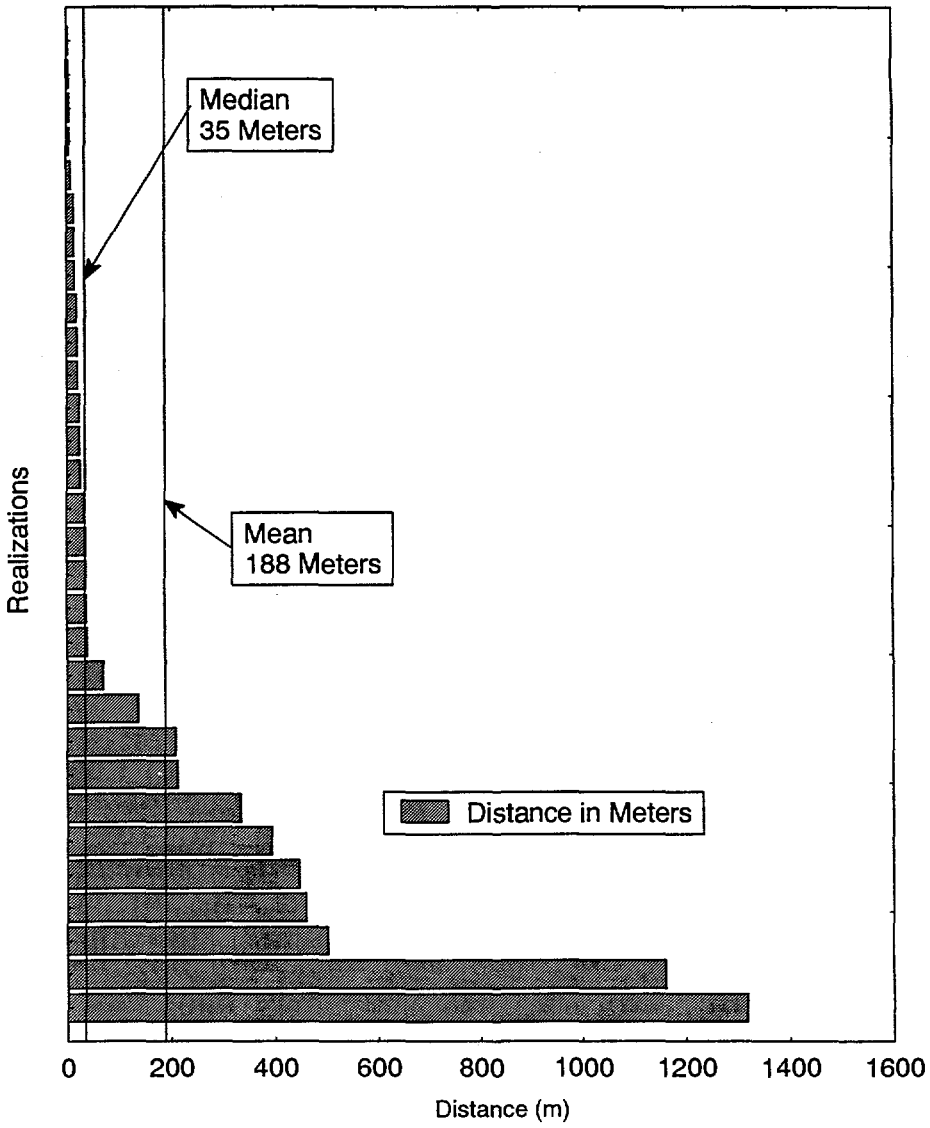

Figure 14. Distances traveled by the centers of mass of 30 plume realizations in 275 years.

between realizations, thereby impacting transport distances. The plume realizations that migrate over very short distances (those traveling less than the median distance) are a result of transport primarily in nonwelded tuff, particularly near the source. In these realizations, the plume did not encounter preferred pathways of flow in the welded tuff, and therefore remained relatively near the source. On the other extreme, plumes that migrate great distances (those traveling longer than the median distance) have clearly encountered well-connected regions of welded tuff having high hydraulic conductivity. Once these preferred paths are entered, the plumes tend to remain in them until a boundary is reached.

Although the travel distances presented above describe the migration of the center of mass of the plume, they do not represent the amount of mass that would actually pass the breakthrough plane

over a given time period. The longer the travel time, the more tritium removed by radioactive decay. The short half-life of tritium causes most of the mass to decay away for travel times to the breakthrough plane of greater than about 200 years. A plot of the breakthrough curves shows that several peaks reach the breakthrough plane before about 100 years (Figure 15a). However, these curves represent less than one-third of the plume realizations, corresponding to the fastest migration rates. Those plumes traveling at lower rates are significantly reduced by radioactive decay and their masses were insufficient to appear on the plot.

The ensemble mean arrival time $\langle t \rangle$ of the peaks of all the plumes that pass the breakthrough plane is 112.5 years. The distribution of the plumes that contributed to this ensemble mean are plotted on Figure 15b. These curves represent the full breakthrough curves obtained by normalizing the decayed breakthrough curves through application of Equation (9). Note that the large range of mean arrival times of individual realizations, from about 50 to about 150 years, results in a very large degree of apparent spreading around $\langle t \rangle$. However, this spreading does not represent the actual spreading of the ensemble plume around $\langle t \rangle$, which is obtained by shifting all the individual normalized breakthrough curves so that they are all centered on $\langle t \rangle$. The results of these shifts, and the corresponding ensemble breakthrough curve, are shown in Figure 15c. The lognormal ensemble breakthrough curve has a standard deviation of 90.3 years.

CONCLUSIONS

The focus of this study was on developing tools for generating maps of hydrogeologic characteristics of the subsurface Tertiary volcanic units at the Frenchman Flat CAU on the NTS.

The first step was to generate the three-dimensional geologic structure for two selected classes: densely welded tuff and nonwelded tuff. The spatial location of possible zones of these selected classes are determined using different geophysical logs available at the NTS. Geophysical log data are widely available on the NTS relative to many other types of geologic and hydrogeologic data. Geophysical logs provide an efficient and cost-effective way of utilizing existing data for delineating the spatial geologic heterogeneity so critical for future flow and transport modeling under the UGTA program.

The second step generated maps of hydraulic conductivity utilizing the spatial distribution of the two geologic classes obtained in the first step. Each class is described by a correlation structure based on existing data on hydraulic conductivity and conditional on the generated spatial location of each class.

The results indicate that the majority of groundwater flow through the volcanic section occurs through zones of densely welded tuff units, where fracturing provides the connectivity pattern. The actual location of each shot and possible existence of welded-tuff regions close to the cavity will determine the potential rate of migration of radionuclides introduced during the nuclear tests. The migration rate is found to range between near zero to approximately four m/yr, with a mean rate of 0.68 m/yr

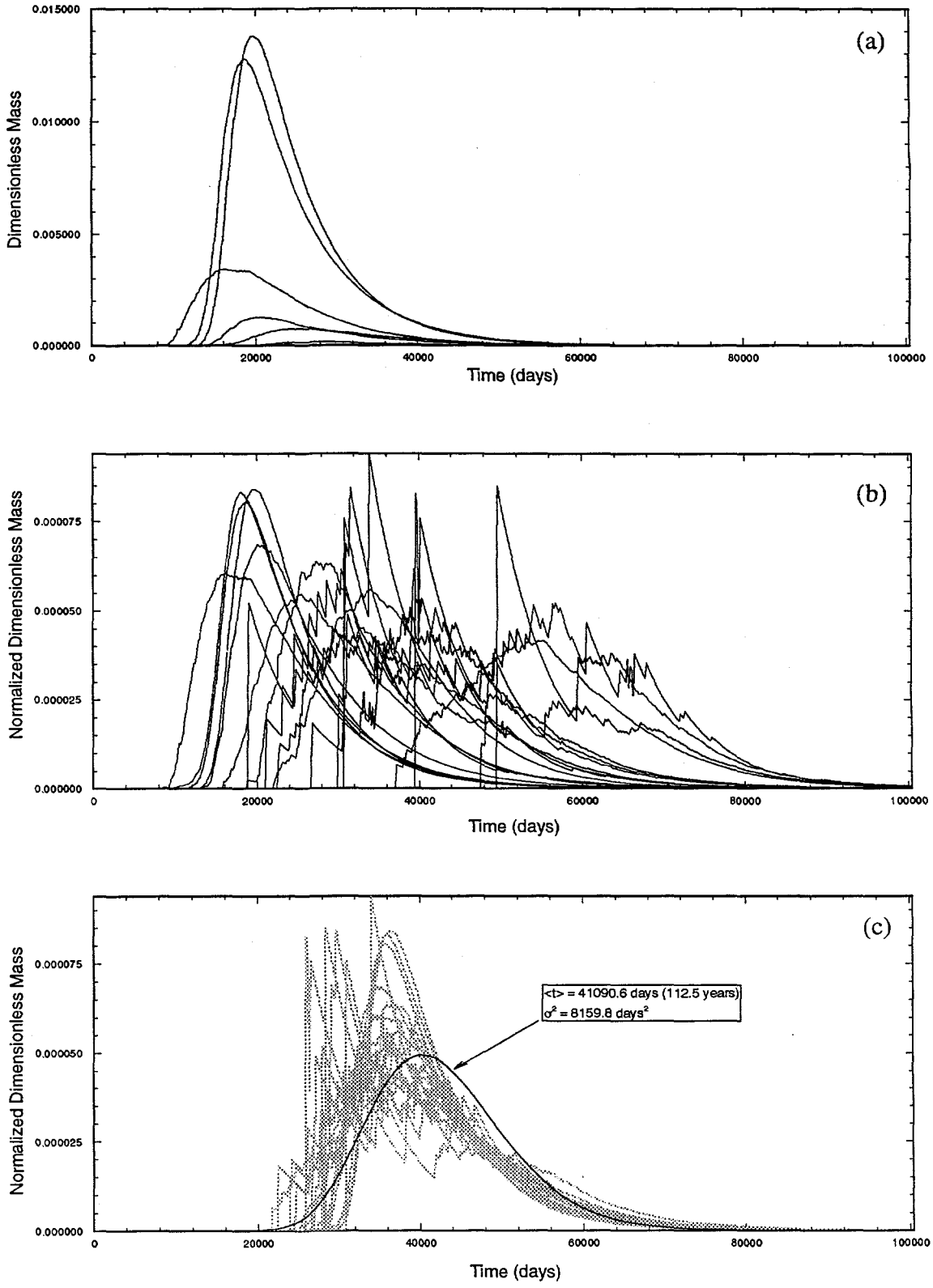

Figure 15. Plots showing (a) tritium breakthrough curves at 500 m downgradient from source, (b) breakthrough curves normalized for tritium decay, and (c) ensemble of breakthrough curves superimposed at mean arrival time of 112.5 years.

Future work should focus on expanding the use of different borehole geophysical tools for delineating the spatial connectivity of important hydrostratigraphic units, including the valley fill and carbonate rocks. Generation of the maps of hydraulic conductivity should serve as a base for applying flow and transport techniques in addressing the issue of possible migration of radionuclides from underground nuclear tests at the NTS. Importantly, the maps can be up scaled appropriately for modeling of areas larger than that modeled in this study.

Pohlmann, K.F. and R. Andricevic, 1994. Identification of Potential Groundwater Flow Paths using Geological and Geophysical Data, Desert Research Institute, Water Resources Center, Publication No. 45128, 23 pp.

Rehfeldt, K., O. Drici, J. Renier, and J. Marie., 1996. Hydrologic Parameter Data Documentation Package, Underground Test Area Subproject, Phase I Data Analysis Task, Volume IV, IT Corporation, prepared for U.S. Dept. of Energy, Env. Rest. Program, 21 p.

Reynolds Electrical and Engineering Co., Inc., Special Projects Section, 1993a. Hydrogeologic Data for Science Trench Boreholes at the Area 5 Radioactive Waste Management Site, Nevada Test Site, Nevada. prepared for the U.S. Dept. of Energy, Nevada Operations Office, variable paging.

Reynolds Electrical and Engineering Co., Inc., Special Projects Section, 1993b. Site Characterization and Monitoring Data from Area 5 Pilot Wells, Nevada Test Site, Nevada. prepared for the U.S. Dept. of Energy, Nevada Operations Office, variable paging.

Shirley, C.T., 1995. Hydrostratigraphic Units within the Alluvium and Tertiary Volcanics of East Central Yucca Flat, Nevada Test Site. M.S. Thesis, Dept. of Geoscience, Univ. of Nevada, Las Vegas, 154 p.

Shirley, S., K.F. Pohlmann, and R. Andricevic, 1996 (in press). Three-Dimensional Mapping of Equiprobable Hydrostratigraphic Units at the Frenchman Flat Corrective Action Unit, Nevada Test Site, Desert Research Institute, Water Resources Center Publication No. 45152.

Tompson, A.F.B. and L.W. Gelhar, 1990. Numerical simulation of solute transport in three-dimensional, randomly heterogeneous porous media, *Water Resources Research*, 26(10), 2541-2562.

Winograd, I.J., and W. Thordarson, 1975. Hydrogeologic and Hydrochemical Framework, South-Central Great Basin, Nevada-California, with Special Reference to the Nevada Test Site, U.S. Geological Survey Professional Paper 712-C, 126 p.

DISTRIBUTION

Bob Bangerter
Environmental Restoration Division
Nevada Operations Office
U.S. Department of Energy
P.O. Box 98518
Las Vegas, NV 89193-8518

Joanne M. Bradbery, Director
Contract Management Division
Nevada Operations Office
U.S. Department of Energy
P.O. Box 98518
Las Vegas, NV 89193-8518

David Bedsun
Defense Special Weapons Agency
Field Command
Nevada Operations Office
P.O. Box 208
Mercury, NV 89023–0208

Beverly Colbert
Contract Management Division
Nevada Operations Office
U.S. Department of Energy
P.O. Box 98518
Las Vegas, NV 89193-8518

Frank Di Sanza, Director
Energy Technologies Division
Nevada Operations Office
U.S. Department of Energy
P.O. Box 98518
Las Vegas, NV 89193-8518

Doug Duncan
Hydrology Program Manager
Environmental Protection Division
Nevada Operations Office
U.S. Department of Energy
P.O. Box 98518
Las Vegas, NV 89193-8518

Dennis Farmer
Radiation Sciences Laboratory
Office of Radiation and Indoor Air
U.S. Environmental Protection Agency
P.O. Box 98517, M/S 513
Las Vegas, NV 89193–8517

Larry Franks
Nevada State Health Department
Radiological Health Section
620 Belrose Avenue
Las Vegas, NV 89158

Joseph M. Ginanni
Waste Management Division
Nevada Operations Office
U.S. Department of Energy
P.O. Box 98518
Las Vegas, NV 89193–8518

Kenneth Hoar, Director
Environmental Protection Division
Nevada Operations Office
U.S. Department of Energy
P.O. Box 98518
Las Vegas, NV 89193-8518

Kathy Izell
Assistant Manager for Technical Services
Nevada Operations Office
U.S. Department of Energy
P.O. Box 98518
Las Vegas, NV 89193-8518

Roger Jacobson
Desert Research Institute
Water Resources Center
P.O. Box 19040
Las Vegas, NV 89132-0040

Marjory Jones
Desert Research Institute
Water Resources Center
P.O. Box 60220
Reno, NV 89506-0220

Jim Kannard
Bechtel Nevada Corporation
P.O. Box 98521
Las Vegas, NV 89193-8521

Randy Laczniak
U.S. Geological Survey
Water Resources Division
6770 S. Paradise Rd.
Las Vegas, NV 89119

Steve Lawrence
Engineering Division
Nevada Operations Office
U.S. Department of Energy
P.O. Box 98518
Las Vegas, NV 89193-8518

Steve Leedom
Stockpile Stewardship Division
Nevada Operations Office
U.S. Department of Energy
P.O. Box 98518
Las Vegas, NV 89193-8518

Charles E. McWilliam, Director
Defense Projects Division
Nevada Operations Office
U.S. Department of Energy
P.O. Box 98518
Las Vegas, NV 89193-8518

Leslie A. Monroe
Environmental Protection Division
Nevada Operations Office
U.S. Department of Energy
P.O. Box 98518
Las Vegas, NV 89193–8518

Ken Ortego
Bechtel Nevada Corporation
P.O. Box 98521
Las Vegas, NV 89193-8521

Ken Rehfeldt
Geotrans, c/o IT
4330 Valley View
Suite 112, MS-439
Las Vegas, NV 89103

David K. Smith
Isotopes Sciences Division
Lawrence Livermore National Laboratory
P.O. Box 808, M/S L231
Livermore, CA 94550

Joe Thompson
Los Alamos National Laboratory
INC-11, MS J514
P.O. Box 1663
Los Alamos, NM 87545

Doug Trudeau
U.S. Geological Survey
Water Resources Division
6770 S. Paradise Rd.
Las Vegas, NV 89119

Janet Wiley
International Technology Corporation
4330 S. Valley View
Suite 114
Las Vegas, NV 89103

Annie Kelley
State Documents Department
Nevada State Library
Capitol Complex
Carson City, NV 89710

Archives
Getchell Library
University of Nevada, Reno

Beverly Carter
MacKay School of Mines Library
University of Nevada, Reno

Document Section, Library
University of Nevada, Las Vegas
4505 Maryland Parkway
Las Vegas, NV 89154

Library (Stead)
Desert Research Institute
P.O. Box 60220
Reno, Nevada 89506–0220

Library
IT Corporation
4330 S. Valley View
Suite 114
Las Vegas, NV 89103
ATTN: Toni Miller

Library
Southern Nevada Science Center
Desert Research Institute
P.O. Box 19040
Las Vegas, NV 89132-0040

Public Reading Facility
Bechtel Nevada Corporation
P.O. Box 98521
Las Vegas, NV 89193-8521

Technical Information Resource Center
Nevada Operations Office
U.S. Department of Energy
P.O. Box 98518
Las Vegas, NV 89193–8518

Librarian
Water Resources Center Archives
410 O'Brien Hall
University of California
Berkeley, CA 94720-1718

Office of Scientific and Technical Information
U.S. Department of Energy
P.O. Box 62
Oak Ridge, TN 37831–9939